nature structural & molecular biology

A cytosolic Ezh1 isoform modulates a PRC2–Ezh1 epigenetic adaptive response in postmitotic cells

Beatrice Bodega[1,8], Federica Marasca[2,7,8], Valeria Ranzani[1], Alessandro Cherubini[1], Francesco Della Valle[3], Maria Victoria Neguembor[4], Michel Wassef[5], Alessio Zippo[1], Chiara Lanzuolo[6], Massimiliano Pagani[1] & Valerio Orlando[2,3]

The evolution of chromatin-based epigenetic cell memory may be driven not only by the necessity for cells to stably maintain transcription programs, but also by the need to recognize signals and allow plastic responses to environmental stimuli. The mechanistic role of the epigenome in adult postmitotic tissues, however, remains largely unknown. In vertebrates, two variants of the Polycomb repressive complex (PRC2–Ezh2 and PRC2–Ezh1) control gene silencing via methylation of histone H3 on Lys27 (H3K27me). Here we describe a reversible mechanism that involves a novel isoform of Ezh1 (Ezh1β). Ezh1β lacks the catalytic SET domain and acts in the cytoplasm of skeletal muscle cells to control nuclear PRC2–Ezh1 activity in response to atrophic oxidative stress, by regulating Eed assembly with Suz12 and Ezh1α (the canonical isoform) at their target genes. We report a novel PRC2–Ezh1 function that utilizes Ezh1β as an adaptive stress sensor in the cytoplasm, thus allowing postmitotic cells to maintain tissue integrity in response to environmental changes.

© 2017 Nature America, Inc., part of Springer Nature. All rights reserved.

In mammals, Polycomb repressive complex (PRC2) exists in two variants, PRC2–Ezh1 and PRC2–Ezh2, that differ in their catalytic components[1–3]. Ezh1 and Ezh2 are oppositely expressed during development and cell differentiation, with Ezh2 predominant in proliferating cells, and Ezh1 predominant in postmitotic tissues[1–9]. Although the function of PRC2–Ezh1 has been investigated in cycling cells, particularly embryonic stem cells[1,2,8,10,11], its role in adult postmitotic tissues remains to be elucidated. Studies involving embryonic totipotent stem cells have suggested that although Ezh1 exerts weak histone methyl transferase (HMTase) activity[1], it substitutes for Ezh2 when the latter is absent, thereby maintaining basal H3K27me3 levels at PRC2 targets[2,8,10,11] and promoting chromatin compaction[1,12]. Recent studies involving differentiating cells suggest that Ezh1 has a role in transcriptional regulation, as it binds promoter regions of active genes, interacts with the transcriptional machinery and remains largely excluded from H3K27me3-repressed domains[3,13–15]. We hypothesized that PRC2–Ezh1 might influence somatic cell biology by modulating gene silencing as part of a cell's adaptive response to environmental stress. To test this hypothesis, we investigated the function of PRC2–Ezh1 in postmitotic mouse skeletal muscle cells.

RESULTS

Ezh1 mediates an increase in H3K27me3 in disuse muscle atrophy

During cell differentiation in C2C12 muscle cells, Ezh1 is upregulated while the global levels of H3K27me3 remain constant, whereas Ezh2 is progressively degraded[3,13] (**Supplementary Fig. 1a**,**b**). To induce a cellular stress response, we treated C2C12 myotubes with a low concentration of H_2O_2 (100 μM) for 24 h, which mimics disuse muscle atrophy in differentiated cells[16,17] without affecting cell viability or inducing a damage response[17] (**Fig. 1a** and **Supplementary Fig. 1c**,**d**); for the opposite condition, we induced myotube hypertrophy via heat-shock treatment (43 °C for 1 h)[18] (**Fig. 1a** and **Supplementary Fig. 1c**). We then analyzed the global H3K27me3 level in normal, atrophic and hypertrophic myotubes. We detected a statistically significant increase in H3K27me3 only in the H_2O_2-treated cells (**Fig. 1a**, **Supplementary Fig. 1e–g** and **Supplementary Data Set 1**). Interestingly, H3K9me3, H3K27me1 and H3K4me3 did not show similar trends (**Supplementary Fig. 1f**), which suggested specific involvement of PRC2. We observed the same effect on H3K27me3 in C2C12 myotubes when we used a different atrophy-inducing agent (100 μM $FeSO_4$ for 24 h)[19] (**Supplementary Fig. 1h**), as well as in human primary myotubes (**Supplementary Fig. 1i**). The increase in H3K27me3 levels did not occur in H_2O_2-treated myotubes depleted of Ezh1 (**Fig. 1b**, **Supplementary Fig. 1j**,**k** and **Supplementary Data Set 1**). Furthermore, we measured Ezh1 and Ezh2 HMTase activity in control and H_2O_2-treated myotubes and found that after atrophic stimulation, the enzymatic activity of Ezh1, but not of Ezh2, increased (**Supplementary Fig. 2a**). Overall, these results indicate that atrophy-like stress elicits a global increase in Ezh1-mediated H3K27me3.

[1]Istituto Nazionale di Genetica Molecolare (INGM) Romeo and Enrica Invernizzi, Milan, Italy. [2]IRCSS Fondazione Santa Lucia, Epigenetics and Genome Reprogramming, Rome, Italy. [3]Environmental Epigenetics Research Program, Division of Biological Environmental Sciences and Engineering, King Abdullah University of Science and Technology (KAUST), Thuwal, Saudi Arabia. [4]Dulbecco Telethon Institute at San Raffaele Scientific Institute, Milan, Italy. [5]Génétique et Biologie du Développement, Institut Curie, Inserm, Paris, France. [6]CNR Institute of Cellular Biology and Neurobiology, Rome, Italy. [7]Present address: Istituto Nazionale di Genetica Molecolare (INGM) Romeo and Enrica Invernizzi, Milan, Italy. [8]These authors contributed equally to this work. Correspondence should be addressed to B.B. (bodega@ingm.org) or V.O. (valerio.orlando@kaust.edu.sa).

Received 16 December 2016; accepted 24 February 2017; published online 27 March 2017; doi:10.1038/nsmb.3392

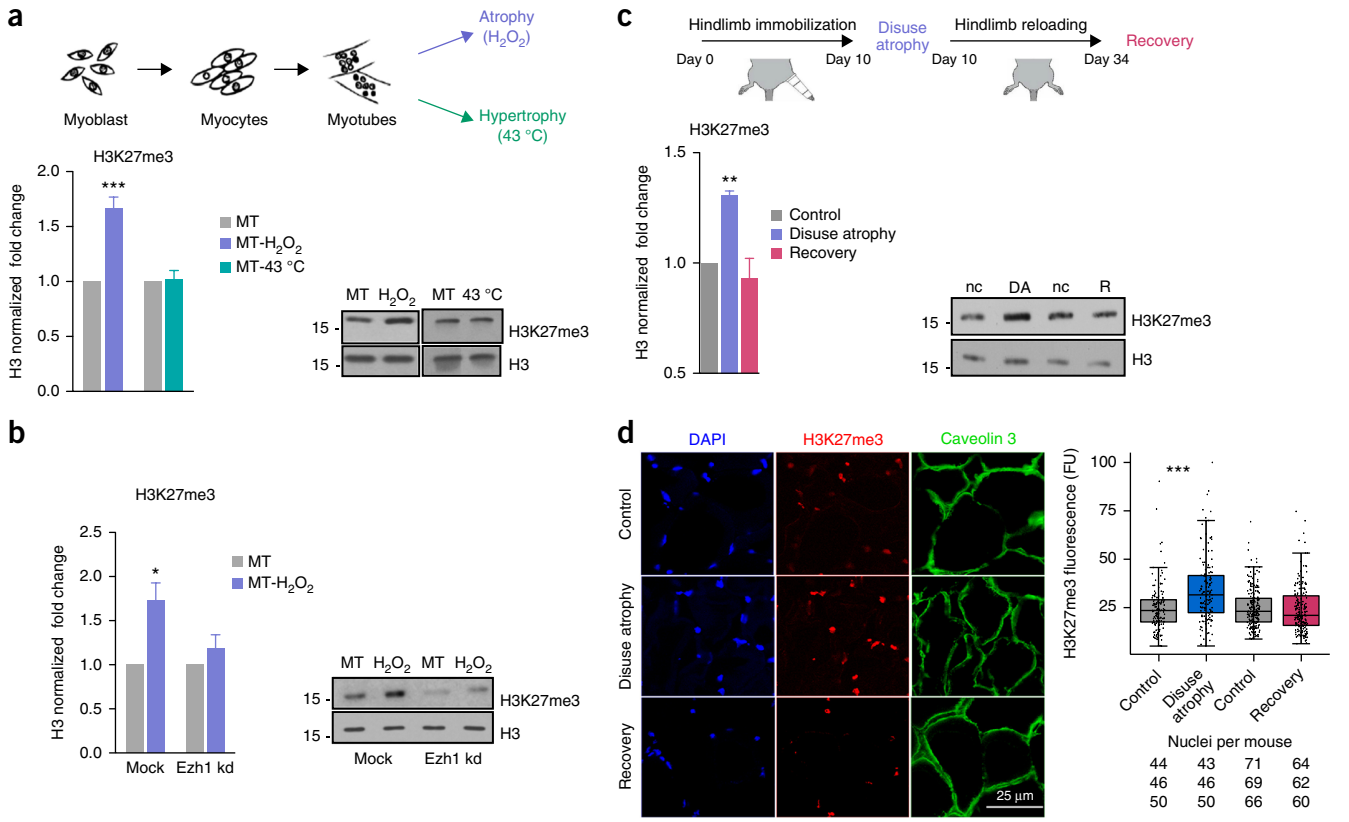

Figure 1 Ezh1 determines the increase in global H3K27me3 levels in disuse muscle atrophy. (**a**) Top, schematic representation of atrophic and hypertrophic phenotypes induced via H_2O_2 and heat-shock (43 °C) treatment, respectively (Online Methods). Bottom, H3K27me3 densitometric quantification and corresponding western blots of histone extracts from control myotubes (MT) and H_2O_2-treated (MT- H_2O_2) or 43 °C heat-shock-treated myotubes (MT-43 °C). Histone H3 was used as the loading control. Data are mean and s.e.m. of $n = 9$ (H_2O_2) or 4 (43 °C) independent experiments. Additional results are shown in **Supplementary Figure 1e**. $^{***}P = 0.0001$, two-tailed paired *t* test, control versus H_2O_2 treatment. (**b**) H3K27me3 densitometric quantification and corresponding western blots of histone extracts from control (mock) and Ezh1-depleted (Ezh1 kd) myotubes treated or not treated with H_2O_2. Histone H3 was used as the loading control. Data are mean and s.e.m. of $n = 3$ independent experiments. Additional results are shown in **Supplementary Figure 1j**. $^{*}P = 0.0315$, one-tailed paired *t* test, control versus H_2O_2 treatment. (**c**) Top, experimental design of disuse atrophy and recovery *in vivo*. Hindlimbs of 3-month-old mice were immobilized in casts for 10 d to stimulate disuse muscle atrophy; after removal of the casts, the hindlimbs were allowed to reload for 24 d to induce recovery of the atrophic phenotype. Bottom, H3K27me3 densitometric quantification and corresponding western blots of histone extracts from tibialis anterior muscles from control (nc), disuse-atrophic (DA) and reloaded (R) mice. Histone H3 was used as the loading control. Data are mean and s.e.m. ($n = 3$ mice); data from individual mice are presented in **Supplementary Figure 2d**. $^{**}P = 0.0031$, two-tailed paired *t* test, control versus disuse atrophy. (**d**) Left, representative immunostaining of transverse sections of tibialis anterior muscle from control, disuse atrophy and reloaded mice ($n = 3$ mice). Nuclei were counterstained with DAPI and stained for H3K27me3 and caveolin 3. Scale bar, 25 µm. Right, corresponding box-and-whisker plot; dots represent integrated fluorescence intensity evaluation. Center bars indicate medians (50% quantile); whiskers represent ±1.5× the interquartile range (IQR); lower and upper hinges indicate the 25% and 75% quantiles, respectively ($n = 3$ mice; the number of nuclei per mouse is shown below the plot). FU, fluorescence units. $^{***}P < 0.0001$, two-tailed unpaired *t* test, control versus disuse atrophy. Uncropped blot images are shown in **Supplementary Data Set 1**. Source data for graphs are available online.

We also used a mouse model of disuse atrophy to investigate whether a similar epigenetic response occurs *in vivo*. We induced disuse muscle atrophy by unilateral hindlimb immobilization[20]. One hindlimb was immobilized by casting for 10 d, and muscles from both hindlimbs were either isolated immediately after removal of the cast or allowed to reload for an additional 24 d (**Fig. 1c**). This process was followed by measurements of cross-sectional area (**Supplementary Fig. 2b**) with increased transcription of *Atrogin1* (*Fbxo32*) and *Murf1* (*Trim63*)—markers of disuse muscle atrophy[21]—and decreased transcription of myosin heavy chain 3 (*Myh3*) (**Supplementary Fig. 2c**). Normal levels of these markers were restored after hindlimb reloading (**Supplementary Fig. 2c**). Notably, the residual level of *Ezh2*, which is present at almost undetectable RNA and protein levels in muscle tissue[4], did not change in atrophic or reloaded muscles (data not shown). In agreement with the data obtained in C2C12 cells (**Fig. 1a**) and consistent with the transcriptional responses of marker genes, western blotting of histone extracts showed a statistically significant increase of the global H3K27me3 level in atrophic muscles (**Fig. 1c**, **Supplementary Fig. 2d** and **Supplementary Data Set 1**); this marker reverted to the control level after hindlimb reloading (**Fig. 1c** and **Supplementary Fig. 2d**). We observed the same trend in C2C12 myotubes when we replaced the H_2O_2 treatment with fresh culture medium (**Supplementary Fig. 2e**,**f**). We then analyzed the presence of H3K27me3 in the nuclei of muscle fibers via immunofluorescence experiments. We observed a significant increase in H3K27me3 fluorescence signals from atrophic muscle fibers compared with those from control and reloaded muscle fibers (**Fig. 1d**). Differences in fluorescence between the control and disuse atrophy samples were not dependent on the areas of the nuclei (**Supplementary Fig. 2g**). These data reveal the specific dynamics of H3K27me3 modification in muscle fibers, and the plastic nature of this epigenetic response.

© 2017 Nature America, Inc., part of Springer Nature. All rights reserved.

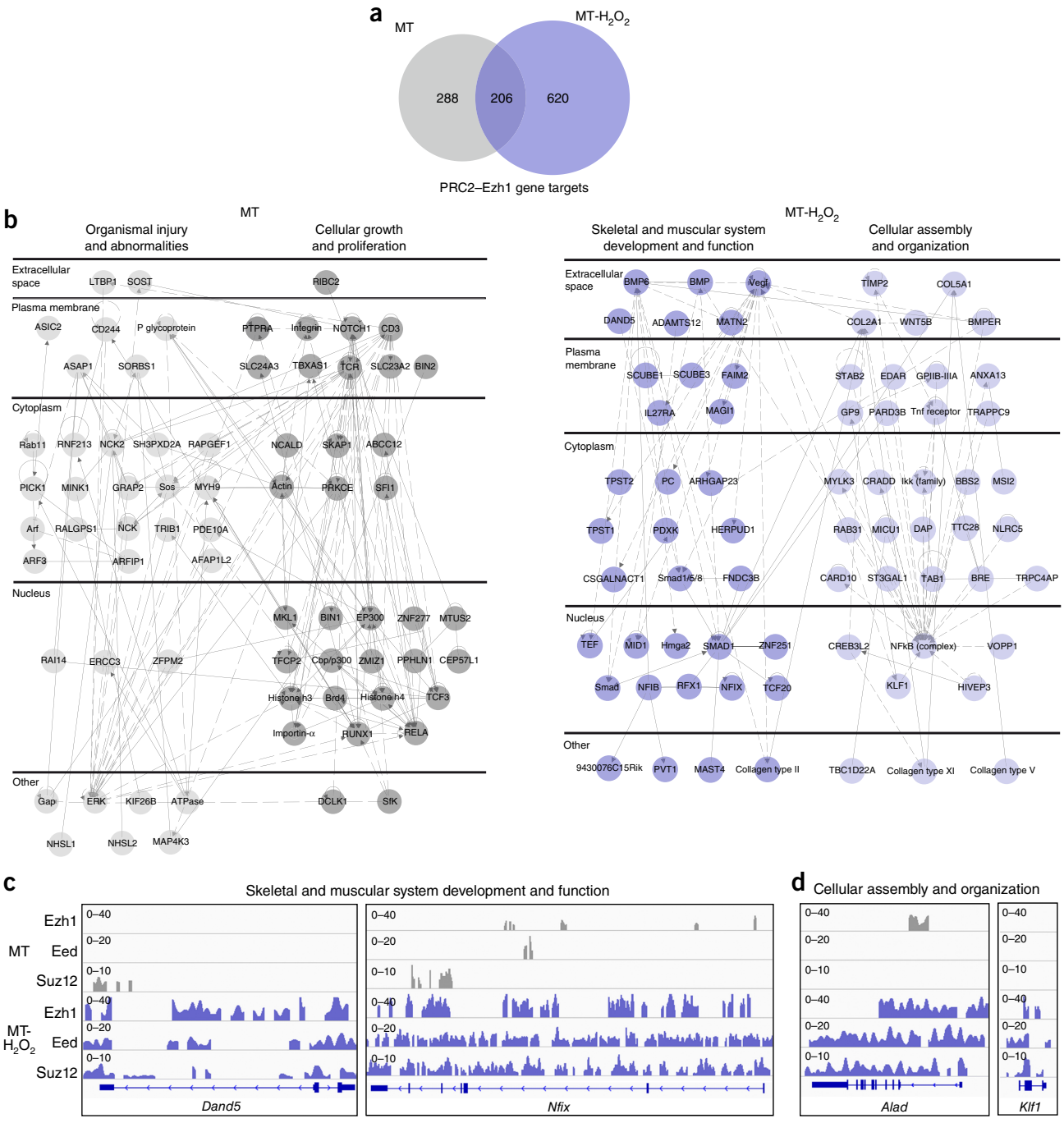

Figure 2 The PRC2–Ezh1 complex is redistributed on muscle-specific targets. (**a**) The overlap between PRC2–Ezh1 target genes (defined as targets of Suz12, Eed and Ezh1 in **Supplementary Fig. 3b**) identified by ChIP-seq analysis in control and H_2O_2-treated myotubes. (**b**) The molecular network of functional relationships extracted from the Ingenuity Pathway Analysis knowledge base for PRC2–Ezh1 gene targets in control and H_2O_2-treated myotubes. Two of the most enriched networks are represented (see also **Supplementary Table 1**). (**c**) Target genes from the "skeletal and muscular system development and function" network reported in **b** (*Dand5* and *Nfix*) were bound by PRC2–Ezh1 complex (Ezh1, Suz12 and Eed) in H_2O_2-treated myotubes but not in controls. (**d**) Target genes from the "cellular assembly and organization" network reported in **b** (*Alad* and *Klf1*) were bound by PRC2–Ezh1 (Ezh1, Suz12 and Eed) in H_2O_2-treated myotubes but not in controls.

PRC2–Ezh1 represses muscle-specific genes after atrophic stress

To link the function of PRC2–Ezh1 to the atrophic phenotype, we carried out genome-wide chromatin immunoprecipitation followed by sequencing (ChIP-seq) of Eed, Suz12 and Ezh1 interpolated with RNA-seq data sets in control and H_2O_2-treated myotubes (the workflow is shown in **Supplementary Fig. 3a**). We identified PRC2–Ezh1's targets as those showing contemporaneous binding of Eed, Suz12 and Ezh1 (**Fig. 2a**, **Supplementary Fig. 3b** and **Supplementary Table 1**). Strikingly, the number of gene targets of PRC2–Ezh1 almost doubled under atrophic conditions (494 versus 826), revealing a considerable genome-wide redistribution of the complex (**Fig. 2a** and **Supplementary Fig. 3c**). To evaluate the phenotypic significance

© 2017 Nature America, Inc., part of Springer Nature. All rights reserved.

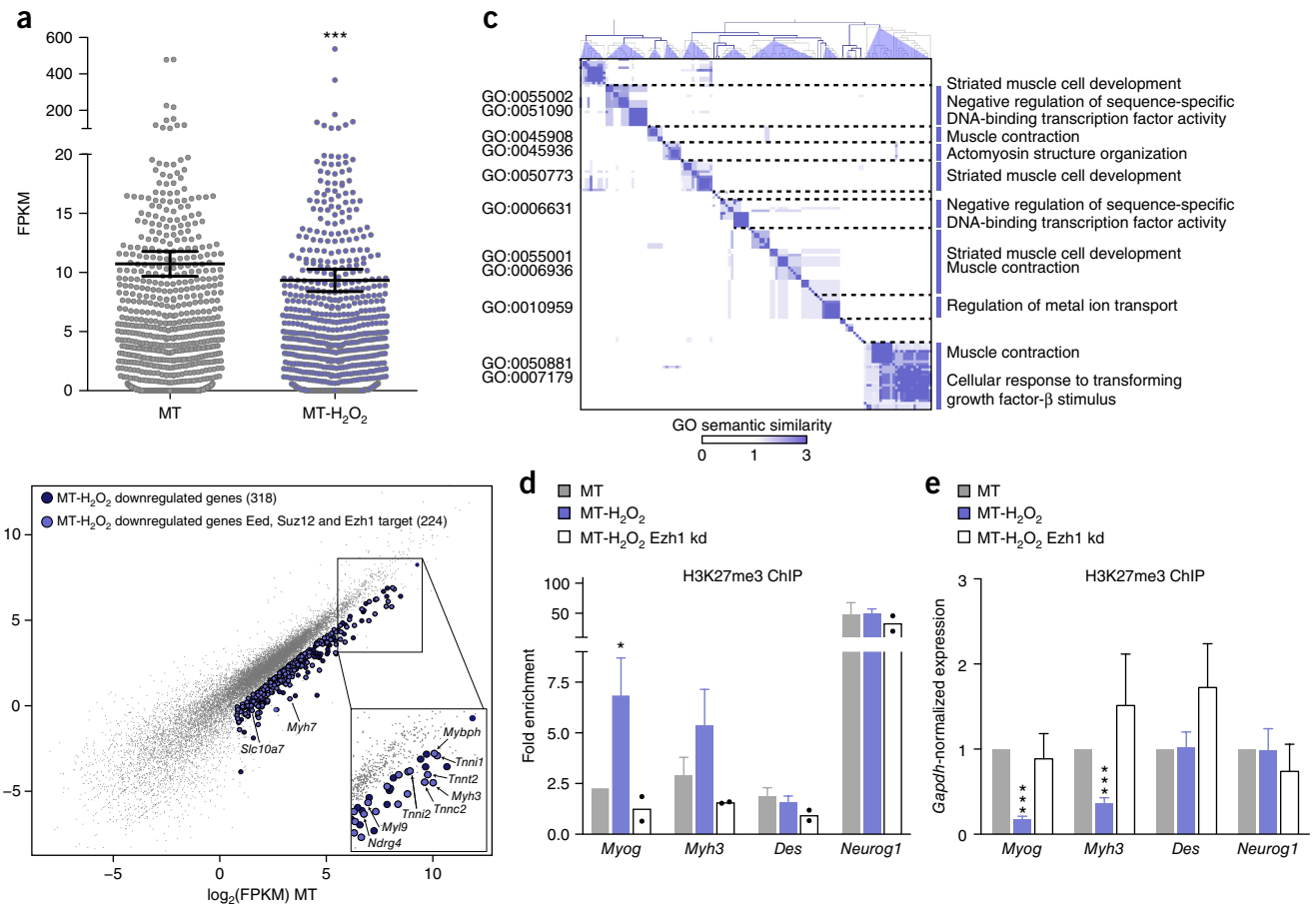

Figure 3 PRC2–Ezh1 is required for the repression of atrophy-related genes after oxidative stress. (**a**) Expression levels (fragments per kilobase of transcript per million mapped reads (FPKM)) of the 826 PRC2–Ezh1 MT-H_2O_2 target genes in control and H_2O_2-treated myotubes. Data are mean ± s.e.m. ***$P < 0.0001$, two-tailed paired *t* test. (**b**) Scatter plot of gene expression in control and H_2O_2-treated myotubes derived from RNA-seq differential expression analysis. Total genes are represented in gray; the 318 downregulated genes in H_2O_2-treated myotubes are in blue ($P < 0.05$, Cuffdiff statistical *t* test; fold change > 2), and 224 of these were Eed, Suz12 and Ezh1 target genes (light blue). Several previously identified[13] Ezh1 targets are highlighted. (**c**) GO semantic similarity matrix of downregulated Eed, Suz12 and Ezh1 target genes in H_2O_2-treated myotubes. The semantic similarity scores of all GO-term pairs were grouped by a hierarchical clustering method with the corresponding cluster representatives (right). The most significant GO terms for each cluster are reported (left; adjusted $P < 0.05$, Fisher's exact test with Benjamini–Hochberg correction). (**d**) H3K27me3 ChIP-qPCR in control myotubes, H_2O_2-treated myotubes, and Ezh1-depleted myotubes treated with H_2O_2 (MT-H_2O_2 Ezh1 kd). Results are represented as fold enrichment over mock (IP control). Data are mean and s.e.m., except when $n = 2$, for which individual values are plotted. $n = 5$ (*Myog*, *Myh3* and *Des* in MT and MT-H_2O_2), 4 (*Neurog1* in MT and MT-H_2O_2) or 2 (MT-H_2O_2 Ezh1 kd) independent experiments. *$P = 0.0411$, one-tailed paired *t* test, *Myog*, MT versus MT-H_2O_2. (**e**) Expression levels of *Myog*, *Myh3*, *Des*, and *Neurog1* in control myotubes, H_2O_2-treated myotubes, and Ezh1-depleted myotubes treated with H_2O_2. Data are normalized to *Gapdh* expression and shown as mean and s.e.m. The number of independent experiments varied depending on the treatment conditions; *Myog*, *Myh3 and Des* were amplified in six or seven independent experiments for MT and MT-H_2O_2 and in four for MT-H_2O_2 Ezh1 kd. *Neurog1* was amplified in three independent experiments for all conditions. ***$P = 8.21913 \times 10^{-6}$ for *Myog*, ***$P = 0.0002$ for *Myh3*, control versus H_2O_2 treatment; two-tailed paired *t* test. Source data for graphs are available online.

of these results, we used Ingenuity Pathway Analysis (**Fig. 2b**). The extracted networks revealed a direct and consistent functional relationship between PRC2–Ezh1 targets in H_2O_2-treated myotubes and the induced atrophic phenotype (**Fig. 2b–d**, **Supplementary Fig. 3d,e** and **Supplementary Table 1**).

RNA-seq analysis indicated that the 826 PRC2–Ezh1 targets in H_2O_2-treated myotubes were significantly repressed compared with control cells (**Fig. 3a**). Moreover, differential expression analysis unveiled a subset of genes (318) that were specifically downregulated after myotube atrophy (**Fig. 3b**). ChIP-seq combined with differential expression analysis indicated high overlap (224 out of 318 (approximately 70%)) among Eed, Suz12 and Ezh1 targets (**Fig. 3b**), including several Ezh1 targets previously reported by Mousavi *et al.*[13] (highlighted in **Fig. 3b**). We carried out Gene Ontology (GO) enrichment analysis and subsequent GO semantic similarity analysis on the 224 protein-coding genes that were downregulated after oxidative stress, and we identified six representative hierarchical cluster terms, again with statistically significant representation of muscle clusters related to the atrophic phenotype (**Fig. 3c**). ChIP-qPCR confirmed that binding of Ezh1, Eed and Suz12 specifically relocalized on selected *Myog* and *Myh3* promoters during myotube atrophy (**Supplementary Fig. 4a**), whereas binding of Ezh2 remained unchanged (**Supplementary Fig. 4b**).

We also observed binding of Ezh1 on muscle gene promoters after the induction of atrophy in a C2C12 cell line that stably expressed hemagglutinin (HA)-tagged Ezh1 protein (**Supplementary Fig. 4c**). We confirmed that H3K27me3 levels were specifically increased on *Myog* and *Myh3* promoters (**Fig. 3d** and **Supplementary Fig. 4d**)

© 2017 Nature America, Inc., part of Springer Nature. All rights reserved.

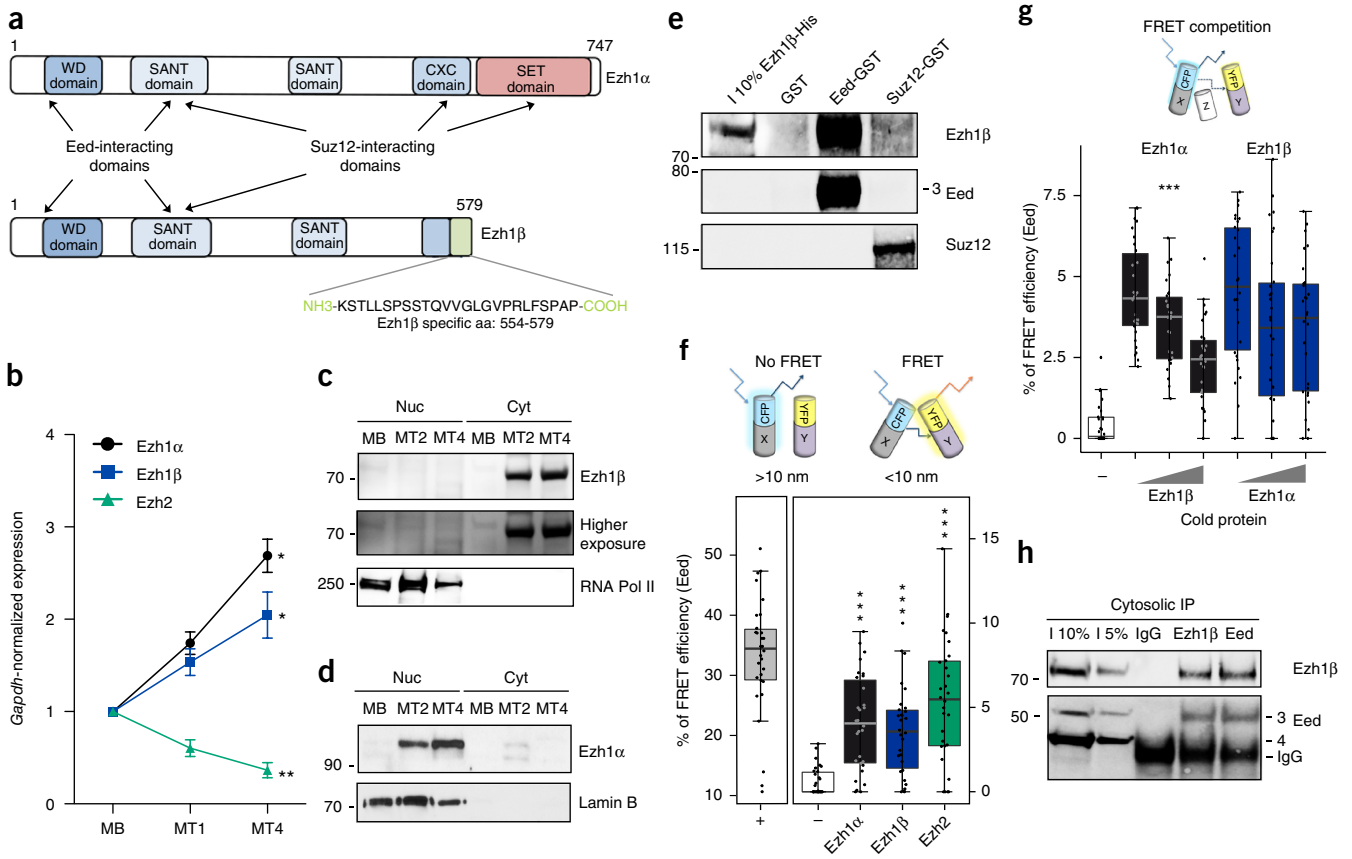

Figure 4 Ezh1 has a cytoplasmic protein isoform, Ezh1β, that interacts with Eed in the cytosolic compartment. (**a**) Schematic representation of the Ezh1α and Ezh1β protein domains[23]; 26 specific amino acids for Ezh1β are highlighted. (**b**) Expression levels of genes encoding Ezh1α, Ezh1β and Ezh2 during C2C12 cell differentiation (MB, myoblasts; MT1, myotubes, day 1; MT4, myotubes, day 4). Data are mean ± s.e.m. of $n = 3$ (Ezh1α) or 4 (Ezh1β and Ezh2) independent experiments. $^{*}P = 0.011$ for Ezh1α, $^{*}P = 0.024$ for Ezh1β, $^{**}P = 0.004$ for Ezh2, MB versus MT4, two-tailed paired *t* test. (**c**,**d**) Western blots of Ezh1β (**c**) and Ezh1α (**d**) during C2C12 myogenic differentiation in nuclear (Nuc) and cytosolic (Cyt) extracts. Lamin B or RNA Pol II was used as the loading control. Data shown are representative of four (Ezh1β) or three (Ezh1α) independent experiments. (**e**) *In vitro* GST pulldown and staining of purified Eed-GST, Suz12-GST and Ezh1β-His-Flag fusion proteins. Anti-GST beads (GST) were used for the negative control. Eed isoform 3 is specified. Data shown are representative of two independent experiments. (**f**) Top, schematic representation of FRET assay of CFP and YFP fusion proteins (CFP-X and YFP-Y). Bottom, box-and-whisker plot; individual points represent the FRET efficiency between YFP-tagged Ezh1α, Ezh1β or Ezh2 and Eed-CFP in NIH/3T3 cells (+, positive control; –, negative control). $n = 3$ independent experiments, with ten nuclei each. $^{***}P < 0.0001$, two-tailed unpaired *t* test versus the negative control. (**g**) Top, schematic representation of FRET competition assay: competition was measured as the reduction in FRET efficiency between CFP-X and YFP-Y due to untagged Z. Bottom, box-and-whisker plot; dots represent the FRET efficiency between YFP-tagged Ezh1α or Ezh1β and Eed-CFP in NIH/3T3 cells cotransfected with increasing amounts of untagged Ezh1β (black) or Ezh1α (blue). In box plots in **f** and **g**, center bars indicate medians (50% quantile); whiskers represent ±1.5× the IQR; lower and upper hinges indicate the 25% and 75% quantiles, respectively. $n = 3$ independent experiments, with ten nuclei each. $^{***}P < 0.0001$, $F = 18.85$, for Ezh1α-Eed in the presence of increasing amounts of cold Ezh1β, one-way analysis of variance (ANOVA) with Bonferroni post-test correction. (**h**) Co-IP and western blots of Ezh1β and Eed in cytosolic extracts of myotubes. Isotype-matched IgG was used as the control antibody. Eed isoforms 3 and 4 are specified. Data shown are representative of two independent experiments. Uncropped blot images are shown in **Supplementary Data Set 1**. Source data for graphs are available online.

concomitantly with their transcriptional repression during myotube atrophy (**Fig. 3e**); knockdown experiments confirmed that Ezh1 was required for the atrophy-induced response, as the analyzed targets no longer exhibited the observed increase in H3K27me3 (**Fig. 3d** and **Supplementary Fig. 4d**) or transcriptional repression (**Fig. 3e**). We confirmed the observed transcriptional repression of the PRC2–Ezh1 targets by inducing myotube atrophy with $FeSO_4$ (**Supplementary Fig. 4e**), and we found that the same genes were upregulated in heat-shock-induced hypertrophy (**Supplementary Fig. 4f**). Notably, gene expression levels were restored to baseline levels when we incubated atrophic myotubes in fresh medium for 48 h (**Supplementary Fig. 4g**), in agreement with our *in vivo* observations (*Myh3*; **Supplementary Fig. 2c**), and indicating the reversibility of oxidative-stress-induced transcriptional repression. Finally, we investigated the possibility that the observed increase in H3K27me3 could be due to the activity of the demethylase Jmjd3 (ref. 22) after oxidative stress. ChIP experiments did not show a reduction in Jmjd3 binding (**Supplementary Fig. 4h**). Overall, these results suggest that after the induction of atrophy, PRC2–Ezh1 redistributes on muscle-specific targets in response to environmental stress.

A novel Ezh1 isoform interacts with Eed in the cytosol of myotubes

We next investigated the mechanism by which PRC2–Ezh1 is activated in response to atrophic stimuli. When we examined *Ezh1* mRNA (http://genome.ucsc.edu; http://www.uniprot.org; http://www.ensembl.org), we noticed the existence of an additional Ezh1 protein-coding transcript annotated in the mouse genome, derived from alternative splicing (UniProt P70351-2). Interestingly, the corresponding protein lacks

© 2017 Nature America, Inc., part of Springer Nature. All rights reserved.

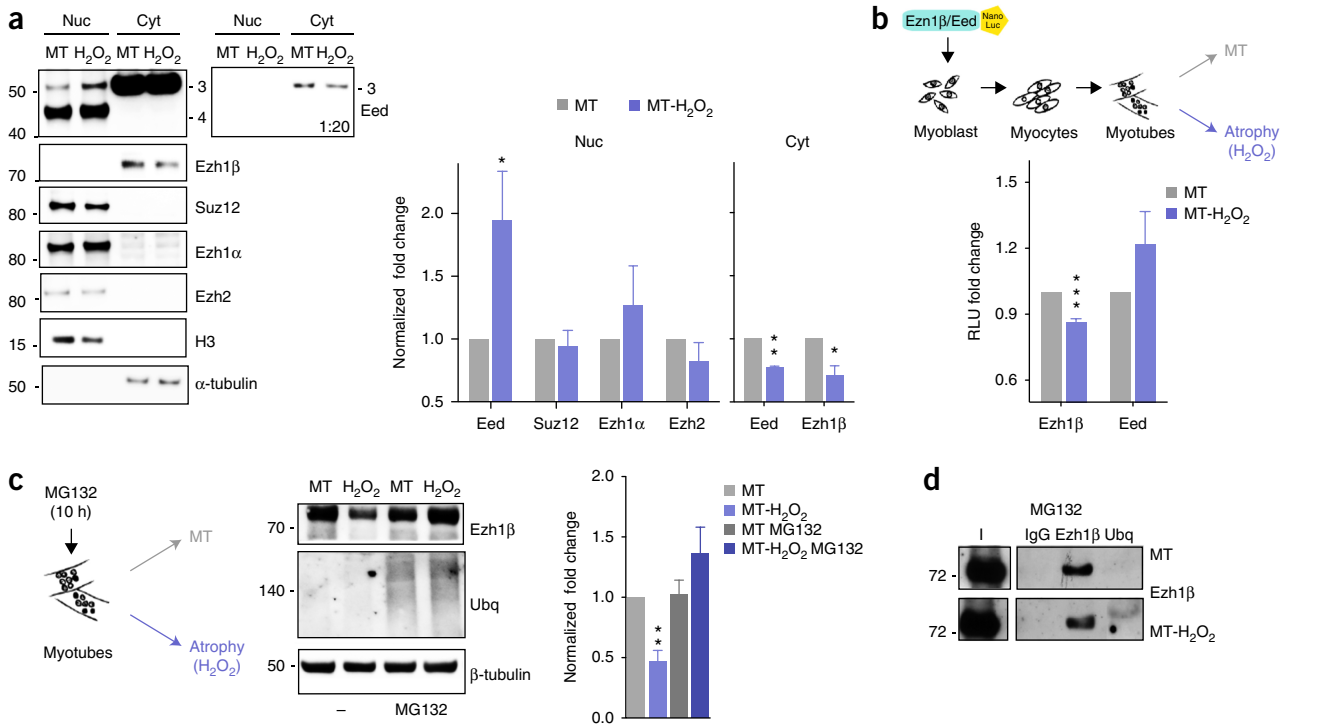

Figure 5 After oxidative stress, Ezh1β is proteolytically degraded while Eed relocalizes from the cytosol to the nucleus. (**a**) Left, western blots showing Eed, Ezh1β, Suz12, Ezh1α and Ezh2 in nuclear (Nuc) and cytosolic (Cyt) extracts of control and H_2O_2-treated myotubes; H3 and α-tubulin were used as loading controls. Eed isoforms 3 and 4 are specified. Right, corresponding densitometric quantification of the nuclear and cytosolic proteins represented on the left. Data are mean and s.e.m. of $n = 4$ (Nuc, except $n = 3$ for Suz12) or 3 (Cyt) independent experiments. $^*P = 0.046$ for Nuc Eed, control versus H_2O_2; $^*P = 0.033$ for Cyt Ezh1β, control versus H_2O_2; one-tailed paired *t* test. $^{**}P = 0.001$ for Cyt Eed, control versus H_2O_2, two-tailed paired *t* test. (**b**) Top, schematic representation of the NanoLuc assay. Eed or Ezh1β open reading frames were cloned in frame with NanoLuc tags. Ezh1β-NanoLuc or Eed-NanoLuc was transfected into C2C12 cells, which were then differentiated and either treated or not treated with H_2O_2. Bottom, luminescence measurements of Ezh1β-NanoLuc and Eed-NanoLuc in control and H_2O_2-treated myotubes. Data represent the fold enrichment over controls; mean and s.e.m. of $n = 5$ (Ezh1β) or 6 (Eed) independent experiments. $^{***}P = 0.0008$, two-tailed paired *t* test versus control. (**c**) Left, schematic representation of MG132 treatment after atrophic stimuli. C2C12 myotubes were treated simultaneously with the proteasome inhibitor MG132 and H_2O_2 for up to 10 h. Middle, western blots showing Ezh1β and ubiquitin (Ubq) in controls and in H_2O_2-, MG132- and MG132-H_2O_2-treated myotubes. β-tubulin was used as the loading control. Right, corresponding densitometric quantification of Ezh1β. Data are mean and s.e.m. of $n = 6$ independent experiments. $^{**}P = 0.002$, two-tailed paired *t* test, H_2O_2 treatment versus control. (**d**) Co-IP and western blots of Ezh1β and ubiquitin in cytosolic extracts of MG132- and MG132-H_2O_2-treated myotubes. Isotype-matched IgG was used as a control antibody. Data are representative of two independent experiments. Uncropped blot images are shown in **Supplementary Data Set 1**. Source data for graphs are available online.

the catalytic SET domain[23] (**Fig. 4a**). We referred to this previously uncharacterized isoform as Ezh1β, and the canonical full-length isoform as Ezh1α. To determine whether myotubes express the alternative spliced isoform, we amplified cDNA with primers for the entire coding region of the Ezh1β gene transcript, and obtained a unique band of 1,740 bp (**Supplementary Fig. 5a**). Sequencing of the band confirmed 100% sequence identity with annotations in the different genomic databases (data not shown). Gene transcripts for Ezh1α and Ezh1β showed concomitant, increased expression during differentiation, contrary to the progressive decline in *Ezh2* expression (**Fig. 4b**). Similarly, the two isoforms were coexpressed in adult mouse tissues (stomach, lung, brain, liver, spleen and skeletal muscle), whereas *Ezh2* was almost undetectable except in the spleen, as previously reported[1] (**Supplementary Fig. 5b**). To investigate the function of Ezh1β, we generated a highly specific polyclonal antibody directed against the Ezh1β C terminus (amino acids 554–579), the only region that was distinct between the two Ezh1 isoforms (**Fig. 4a**). We assessed the specificity of the antibody to the Ezh1β C terminus by using NIH/3T3 cells that overexpressed either Ezh1α-YFP or Ezh1β-YFP in both western blotting and immunoprecipitation (IP) assays (**Supplementary Fig. 5c,d**). Strikingly, we found that Ezh1β was localized in the cytosol of differentiated muscle cells (**Fig. 4c**). To exclude cross-reactivity with Ezh1α, we used an antibody from R. Margueron's lab[1] (**Supplementary Fig. 5e**) and confirmed that this isoform was located exclusively in the nucleus (**Fig. 4d** and **Supplementary Fig. 1a**).

Given that Ezh1β retains several of the motifs needed for interaction with the PRC2 core components (i.e., Suz12 and Eed) (**Fig. 4a**), we took advantage of *in vitro* assays to measure direct interactions between Ezh1β and Eed or Suz12. GST pulldown assays revealed Ezh1β-Eed interaction rather than Ezh1β-Suz12 interaction (**Fig. 4e** and **Supplementary Data Set 1**). Further, fluorescence resonance energy transfer (FRET) experiments showed that Eed interacted directly with Ezh2, Ezh1α and Ezh1β with similar affinities (**Fig. 4f**). Given that Ezh1α and Ezh1β are coexpressed during muscle differentiation, we carried out a FRET competition assay to test their reciprocal affinity for Eed (**Fig. 4g**). We found that Ezh1β was able to compete with Ezh1α with greater affinity for Eed in a linearly dosage-dependent manner (**Fig. 4g**), whereas the competition in the opposite direction (Ezh1α competing with Ezh1β for Eed interaction) did not show the same efficiency (**Fig. 4g**). Intriguingly, co-IP experiments on cytosolic or nuclear extracts showed that the Eed-Ezh1β interaction took place in the cytosol of differentiated myotubes (**Fig. 4h**,

© 2017 Nature America, Inc., part of Springer Nature. All rights reserved.

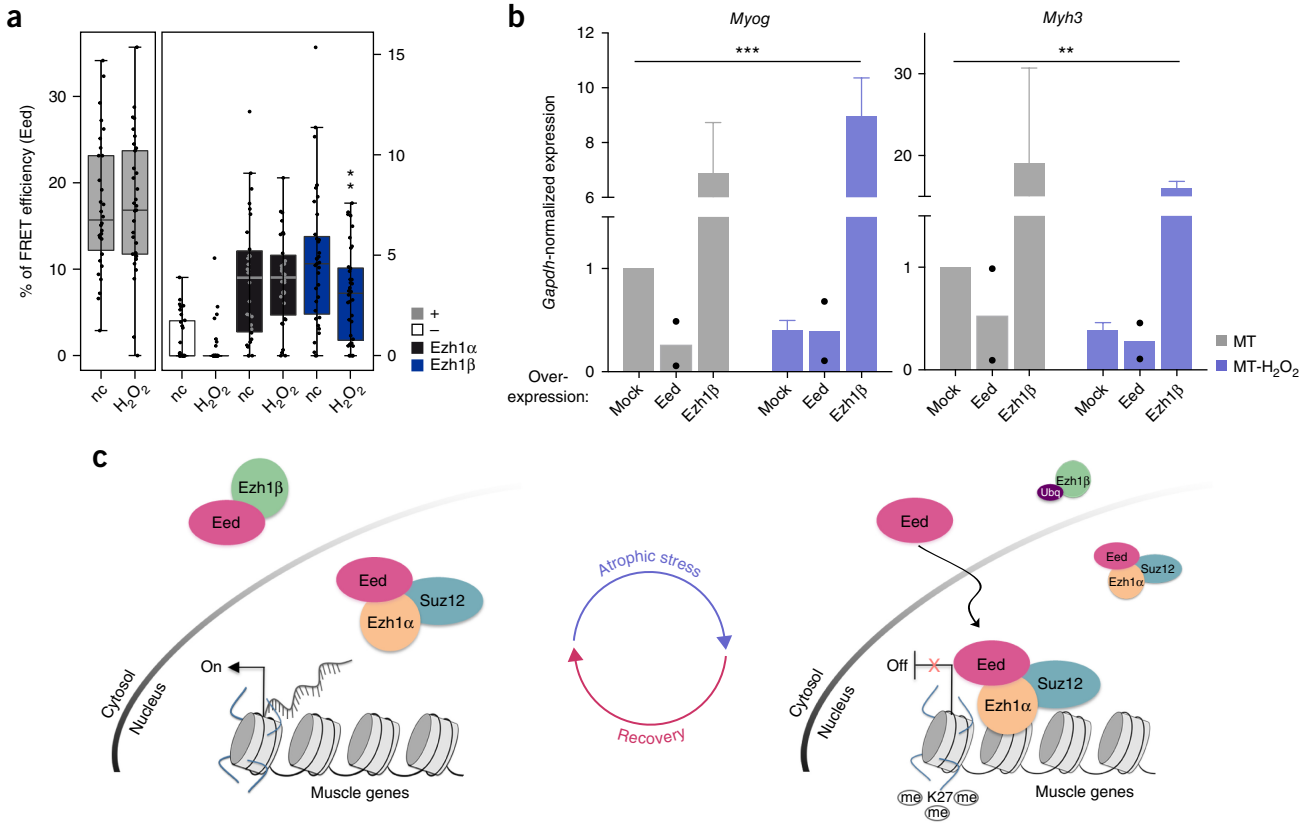

Figure 6 Ezh1β counterbalances PRC2–Ezh1's nuclear assembly and repressive function on target genes. (**a**) Box-and-whisker plot of FRET efficiency; individual points represent FRET efficiency between YFP-tagged Ezh1α or Ezh1β and Eed-CFP in control or H_2O_2-treated NIH/3T3 cells (+, YFP fused to CFP, positive control; –, YFP and Eed-CFP, negative control). Center bars indicate medians (50% quantile); whiskers represent ±1.5× the IQR; lower and upper hinges indicate 25% and 75% quantiles, respectively. $n = 3$ independent experiments, with 10–12 nuclei per experiment. $^{**}P = 0.0095$, one-tailed unpaired t test, Ezh1β control (nc) versus H_2O_2 treatment. (**b**) Expression levels of *Myog* and *Myh3* in myotubes transfected with mock (empty vector), Ezh1β or Eed, treated or not treated with H_2O_2. Data are mean and s.e.m., except when $n = 2$, for which individual values are plotted. $n = 3$ independent experiments, except for Eed ($n = 2$) and mock ($n = 4$). $^{***}P < 0.0001$, $F = 39.41$; $^{**}P = 0.005$, $F = 8.499$; two-way ANOVA with Bonferroni post-test correction. Source data for graphs are available online. (**c**) Schematic model of cytosolic Ezh1β function in postmitotic differentiated muscle cells. Cytosolic Ezh1β maintains the balance of the cytosolic-nuclear distribution of Eed. As a consequence of the Ezh1β-Eed cytosolic interaction, Eed assembly in functional PRC2–Ezh1 complexes is prevented, and thus target gene expression is regulated. After oxidative stress induction, Ezh1β undergoes proteosomal degradation, which changes the Eed cytosolic-nuclear distribution and allows Eed nuclear relocalization and assembly with the rest of the PRC2–Ezh1α complex on chromatin to repress muscle targets, consistent with an atrophic phenotype.

© 2017 Nature America, Inc., part of Springer Nature. All rights reserved.

Supplementary Fig. 5f and **Supplementary Data Set 1**). In agreement with GST pulldown results, we did not detect any interaction between Suz12 and Ezh1β in the cytosol or the nucleus (**Fig. 4e** and **Supplementary Fig. 5g**). We thus hypothesized that the Eed-Ezh1β cytosolic interaction could be involved in the modulation of stress-induced nuclear redistribution and gene silencing of PRC2–Ezh1.

Ezh1β levels control nuclear PRC2–Ezh1 assembly and function

The presence of Eed in the cytosol was reported previously[24,25], although its function was not elucidated (Eed knockdown experiments confirmed the fidelity of the bands revealed in western blotting experiments; **Supplementary Fig. 6a**). We found that two of the four Eed isoforms (isoforms 3 and 4)[26] were expressed in C2C12 myotubes, with isoform 3 being predominantly cytosolic and redistributing from cytosol to nucleus in atrophic myotubes (**Fig. 5a**, **Supplementary Data Set 1** and **Supplementary Fig. 6b**,**c**). Moreover, we found that the amount of cytosolic Ezh1β decreased after stress induction (**Fig. 5a**), whereas the amounts of Suz12, Ezh1α and Ezh2 remained unchanged (**Fig. 5a**, **Supplementary Fig. 6b**,**c** and **Supplementary Data Set 1**).

Moreover, fluorescence correlation analysis and proximity ligation assay of coimmunostained Eed–Suz12 revealed an increased association between the two PRC2 core components in the nuclei of atrophic myotubes (**Supplementary Fig. 6b**,**d**,**e**).

Given that oxidative atrophic stress activates the proteasome pathway[27], we hypothesized that the observed reduction in Ezh1β protein levels (**Fig. 5a**) could be due to proteasomal degradation. First, we checked the stability of Ezh1β by luciferase reporter assay (**Fig. 5b**). We fused a NanoLuc reporter to Ezh1β (or to Eed as a control), and we transfected the reporter into C2C12 and NIH/3T3 cells. We observed that the stability of Ezh1β, but not of Eed, was reduced after H_2O_2 treatment in both cellular systems (**Fig. 5b** and **Supplementary Fig. 6f**). Then we checked the stability of Ezh1β and other PRC2 proteins in atrophic myotubes in the presence of the proteasome inhibitor MG132. After treatment with H_2O_2 combined with MG132, only the Ezh1β levels were restored (**Fig. 5c** and **Supplementary Data Set 1**), whereas levels of Eed, Suz12 and Ezh1α remained unaffected (**Supplementary Fig. 6g**). We observed the same result in NIH/3T3 cells treated with H_2O_2 (**Supplementary Fig. 6h**). IP with anti-ubiquitin confirmed increased polyubiquitylation of Ezh1β in H_2O_2-treated

© 2017 Nature America, Inc., part of Springer Nature. All rights reserved.

myotubes (**Fig. 5d**, **Supplementary Fig. 6i** and **Supplementary Data Set 1**). Notably, in agreement with the reduced stability of Ezh1β under atrophic conditions, FRET experiments conducted under stress conditions showed that interaction between Eed and Ezh1β was reduced after H_2O_2 treatment (**Fig. 6a**). We hypothesized that in normal conditions Ezh1β would hold Eed in the cytosol, thereby controlling its levels in the nucleus and consequently on chromatin, and modulating stress-induced PRC2–Ezh1-mediated gene silencing. Thus, we perturbed the system by overexpressing Eed or Ezh1β in control and H_2O_2-treated myotubes (**Supplementary Fig. 6j**) and analyzed the expression of the PRC2–Ezh1 targets *Myog* and *Myh3* (**Fig. 6b**). As expected, we observed that muscle genes were repressed only in atrophic stress. Conversely, when Eed was overexpressed, the same targets were repressed in both untreated and treated myotubes. Finally, when Ezh1β was overexpressed, the targets were upregulated in both untreated and treated myotubes (**Fig. 6b**). Thus the levels of Eed and Ezh1β influence gene transcription in opposite ways, either enhancing or preventing gene silencing, which suggests that fine-tuning of PRC2–Ezh1 is instrumental in the regulation of gene expression in both normal and stress conditions.

DISCUSSION

Here we describe Ezh1β, a cytosolic Ezh1 isoform that is coexpressed with nuclear Ezh1α. Indeed, some evidence suggests that PRC2 proteins have extranuclear functions[28–33], mainly linked to signal transduction. Cytosolic localization of Eed has been observed in the plasma membrane after integrin activation[24] and in response to tumor necrosis factor[25], promoting coordination between the signaling pathway and transcriptional derepression[24]. We propose that Ezh1β acts as an adaptive environmental 'sensor' that controls the epigenome's structure by retaining Eed in the cytosol to prevent its assembly in the functional PRC2–Ezh1 complex (**Fig. 6c**). The lack of balance below the threshold of Ezh1β availability, owing to its sensitivity to the environment, may indicate PRC2 remodeling, particularly the distribution of Eed from the cytosol to the nucleus; this event would favor increased PRC2–Ezh1α formation at target sites in the nucleus, and prime an epigenetic response to protect cell integrity and the acquisition of the atrophic phenotype (**Fig. 6c**). After removal of the atrophic stimuli both *in vitro* and *in vivo*, H3K27me3 levels and muscle gene expression were restored to physiological conditions, which indicates a plastic and reversible property mediated by the Polycomb memory system. Skeletal muscle is flexible and easily molded, depending on the stimulation (e.g., exercise, inactivity, diet or hormones)[34]. Myofibers must react promptly to the environment by adapting the muscle's metabolic and structural state through specific transcriptional programs. In this context, the capability to recover the physiological phenotype is intrinsic to this transcriptional plasticity. Different types of muscle atrophy have been reported to share a common set of transcriptionally regulated genes[21]. In particular, genes involved in muscle growth and differentiation are mainly repressed under atrophic conditions, whereas genes encoding protein ubiquitylation and degradation are upregulated (atrogenes). Among these genes, *Ezh1* was found to be overexpressed, which suggests its involvement in silenced chromatin formation[21].

In mammalian cells, different PRC2 complexes arise from the combination of alternative elements. Two paralog genes encode Ezh1 and Ezh2 as evolutionary variants of the *Drosophila Ez* gene, and alternative translation sites produce four different Eed isoforms[26]. Among the different isoforms of Eed, only two are expressed in differentiating cells: isoform 3 (50 kDa) and, to a lesser extent, isoform 4 (around 40 kDa)[35], as we detected in C2C12 myotubes (**Fig. 5a** and **Supplementary Fig. 6a**). In our work, we focused our attention on Eed isoform 3, given its peculiar cytosolic and nuclear distribution. The functions of different Eed isoforms are still elusive[26,36,37], and further investigation will be required to determine potential Eed-isoform-specific functions.

The estimated number of transcripts for each transcriptional unit potentially translated increases[38] in the evolutionary scale. In this context the increasing complexity of splicing variants in evolution for many chromatin remodelers is intriguing. Others have reported the existence of two *Ezh2* splicing variants, occupying different subsets of genes in epithelial cells[39]. Indeed, human *EZH1* has a higher number of predicted coding transcripts (at least five) than the corresponding mouse locus. As with transcription factors, it is becoming evident that the activity of epigenome machineries may be regulated by protein-protein interactions, depending on the combinatorial events, possibly in different cellular compartments.

Here we describe a novel role for the Polycomb memory system, which controls phenotypic variation by directly constraining environmental signals from the cytoplasm to chromatin, suggesting that this evolutionary mechanism of fine protein diversification has evolved to control a plethora of multifaceted epigenetic responses necessary to allow complex organisms to adapt to the environment.

METHODS

Methods, including statements of data availability and any associated accession codes and references, are available in the online version of the paper.

Note: Any Supplementary Information and Source Data files are available in the online version of the paper.

ACKNOWLEDGMENTS

We are grateful to C. Desplan, P. Sassone-Corsi, D. Gabellini, E. Battaglioli and S. Biffo for discussions and critical revision of the manuscript; G. Natoli (IFOM-IEO Campus, Milan, Italy) for sharing the Jmjd3 antibody; M. Mora ("Cells, tissues and DNA from patients with neuromuscular diseases" Telethon Biobank, Milan, Italy) for providing human primary myoblasts; R. Margueron (Institute Curie, Paris, France) for providing pCDNA-4TO-Ezh1α-HA plasmid; Sequentia Biotech SL, R. Bonnal and C. Cheroni for bioinformatical support; and M. Moro and M.C. Crosti for technical assistance with cell sorting. This work was supported by the EPIGEN Italian flagship program and King Abdullah University of Science and Technology (KAUST) (to V.O.).

AUTHOR CONTRIBUTIONS

B.B. conceived the study, designed and performed experiments, analyzed the data and wrote the manuscript. F.M. designed and performed experiments, analyzed the data and wrote the manuscript. V.R. performed RNA-seq and ChIP-seq analyses. A.C. set up, performed and analyzed FRET and GST pulldown biochemical assays. F.D.V. performed and analyzed immunofluorescence assays and set up the *in vivo* model of atrophy. M.V.N. set up the protocol for obtaining histone extracts from muscle tissue. M.W. produced and shared the Ezh1α antibody (Margueron lab). A.Z. conceived and analyzed FRET and GST pulldown biochemical assays. C.L. conceived and analyzed immunofluorescence assays and carried out data analyses. M.P. conceived and analyzed RNA-seq and ChIP-seq analyses, and provided technical support for Ezh1β-C antibody design and the western blotting setup. V.O. conceived the study, designed experiments, analyzed the data and wrote the manuscript.

COMPETING FINANCIAL INTERESTS

The authors declare no competing financial interests.

Reprints and permissions information is available online at http://www.nature.com/reprints/index.html.

1. Margueron, R. *et al*. Ezh1 and Ezh2 maintain repressive chromatin through different mechanisms. *Mol. Cell* **32**, 503–518 (2008).
2. Shen, X. *et al*. EZH1 mediates methylation on histone H3 lysine 27 and complements EZH2 in maintaining stem cell identity and executing pluripotency. *Mol. Cell* **32**, 491–502 (2008).

3. Stojic, L. *et al.* Chromatin regulated interchange between Polycomb repressive complex 2 (PRC2)-Ezh2 and PRC2-Ezh1 complexes controls myogenin activation in skeletal muscle cells. *Epigenetics Chromatin* **4**, 16 (2011).
4. Laible, G. *et al.* Mammalian homologues of the Polycomb-group gene Enhancer of zeste mediate gene silencing in *Drosophila* heterochromatin and at *S. cerevisiae* telomeres. *EMBO J.* **16**, 3219–3232 (1997).
5. Bracken, A.P. *et al.* EZH2 is downstream of the pRB-E2F pathway, essential for proliferation and amplified in cancer. *EMBO J.* **22**, 5323–5335 (2003).
6. Caretti, G., Di Padova, M., Micales, B., Lyons, G.E. & Sartorelli, V. The Polycomb Ezh2 methyltransferase regulates muscle gene expression and skeletal muscle differentiation. *Genes Dev.* **18**, 2627–2638 (2004).
7. Ezhkova, E. *et al.* EZH1 and EZH2 cogovern histone H3K27 trimethylation and are essential for hair follicle homeostasis and wound repair. *Genes Dev.* **25**, 485–498 (2011).
8. Hidalgo, I. *et al.* Ezh1 is required for hematopoietic stem cell maintenance and prevents senescence-like cell cycle arrest. *Cell Stem Cell* **11**, 649–662 (2012).
9. Henriquez, B. *et al.* Ezh1 and Ezh2 differentially regulate PSD-95 gene transcription in developing hippocampal neurons. *Mol. Cell. Neurosci.* **57**, 130–143 (2013).
10. Ezhkova, E. *et al.* Ezh2 orchestrates gene expression for the stepwise differentiation of tissue-specific stem cells. *Cell* **136**, 1122–1135 (2009).
11. Fragola, G. *et al.* Cell reprogramming requires silencing of a core subset of polycomb targets. *PLoS Genet.* **9**, e1003292 (2013).
12. Son, J., Shen, S.S., Margueron, R. & Reinberg, D. Nucleosome-binding activities within JARID2 and EZH1 regulate the function of PRC2 on chromatin. *Genes Dev.* **27**, 2663–2677 (2013).
13. Mousavi, K., Zare, H., Wang, A.H. & Sartorelli, V. Polycomb protein Ezh1 promotes RNA polymerase II elongation. *Mol. Cell* **45**, 255–262 (2012).
14. Riising, E.M. & Helin, K. A new role for the polycomb group protein Ezh1 in promoting transcription. *Mol. Cell* **45**, 145–146 (2012).
15. Xu, J. *et al.* Developmental control of polycomb subunit composition by GATA factors mediates a switch to non-canonical functions. *Mol. Cell* **57**, 304–316 (2015).
16. McClung, J.M., Judge, A.R., Talbert, E.E. & Powers, S.K. Calpain-1 is required for hydrogen peroxide-induced myotube atrophy. *Am. J. Physiol. Cell Physiol.* **296**, C363–C371 (2009).
17. Siu, P.M., Wang, Y. & Alway, S.E. Apoptotic signaling induced by H_2O_2-mediated oxidative stress in differentiated C2C12 myotubes. *Life Sci.* **84**, 468–481 (2009).
18. Szustakowski, J.D. *et al.* Dynamic resolution of functionally related gene sets in response to acute heat stress. *BMC Mol. Biol.* **8**, 46 (2007).
19. Gomes-Marcondes, M.C. & Tisdale, M.J. Induction of protein catabolism and the ubiquitin-proteasome pathway by mild oxidative stress. *Cancer Lett.* **180**, 69–74 (2002).
20. Kazi, A.A., Hong-Brown, L., Lang, S.M. & Lang, C.H. Deptor knockdown enhances mTOR activity and protein synthesis in myocytes and ameliorates disuse muscle atrophy. *Mol. Med.* **17**, 925–936 (2011).
21. Lecker, S.H. *et al.* Multiple types of skeletal muscle atrophy involve a common program of changes in gene expression. *FASEB J.* **18**, 39–51 (2004).
22. De Santa, F. *et al.* The histone H3 lysine-27 demethylase Jmjd3 links inflammation to inhibition of polycomb-mediated gene silencing. *Cell* **130**, 1083–1094 (2007).
23. Ciferri, C. *et al.* Molecular architecture of human polycomb repressive complex 2. *eLife* **1**, e00005 (2012).
24. Witte, V. *et al.* HIV-1 Nef mimics an integrin receptor signal that recruits the polycomb group protein Eed to the plasma membrane. *Mol. Cell* **13**, 179–190 (2004).
25. Philipp, S. *et al.* The Polycomb group protein EED couples TNF receptor 1 to neutral sphingomyelinase. *Proc. Natl. Acad. Sci. USA* **107**, 1112–1117 (2010).
26. Kuzmichev, A., Jenuwein, T., Tempst, P. & Reinberg, D. Different EZH2-containing complexes target methylation of histone H1 or nucleosomal histone H3. *Mol. Cell* **14**, 183–193 (2004).
27. Tawa, N.E. Jr., Odessey, R. & Goldberg, A.L. Inhibitors of the proteasome reduce the accelerated proteolysis in atrophying rat skeletal muscles. *J. Clin. Invest.* **100**, 197–203 (1997).
28. Prinjha, R. & Tarakhovsky, A. Chromatin targeting drugs in cancer and immunity. *Genes Dev.* **27**, 1731–1738 (2013).
29. Su, I.H. *et al.* Polycomb group protein Ezh2 controls actin polymerization and cell signaling. *Cell* **121**, 425–436 (2005).
30. Gunawan, M. *et al.* The methyltransferase Ezh2 controls cell adhesion and migration through direct methylation of the extranuclear regulatory protein talin. *Nat. Immunol.* **16**, 505–516 (2015).
31. Bryant, R.J., Winder, S.J., Cross, S.S., Hamdy, F.C. & Cunliffe, V.T. The Polycomb Group protein EZH2 regulates actin polymerization in human prostate cancer cells. *Prostate* **68**, 255–263 (2008).
32. Natsume, A. *et al.* Chromatin regulator PRC2 is a key regulator of epigenetic plasticity in glioblastoma. *Cancer Res.* **73**, 4559–4570 (2013).
33. Roy, A., Basak, N.P. & Banerjee, S. Notch1 intracellular domain increases cytoplasmic EZH2 levels during early megakaryopoiesis. *Cell Death Dis.* **3**, e380 (2012).
34. Sandri, M. Signaling in muscle atrophy and hypertrophy. *Physiology (Bethesda)* **23**, 160–170 (2008).
35. Kuzmichev, A. *et al.* Composition and histone substrates of polycomb repressive group complexes change during cellular differentiation. *Proc. Natl. Acad. Sci. USA* **102**, 1859–1864 (2005).
36. Montgomery, N.D., Yee, D., Montgomery, S.A. & Magnuson, T. Molecular and functional mapping of EED motifs required for PRC2-dependent histone methylation. *J. Mol. Biol.* **374**, 1145–1157 (2007).
37. Montgomery, N.D. *et al.* The murine polycomb group protein Eed is required for global histone H3 lysine-27 methylation. *Curr. Biol.* **15**, 942–947 (2005).
38. Djebali, S. *et al.* Landscape of transcription in human cells. *Nature* **489**, 101–108 (2012).
39. Grzenda, A. *et al.* Functional characterization of EZH2β reveals the increased complexity of EZH2 isoforms involved in the regulation of mammalian gene expression. *Epigenetics Chromatin* **6**, 3 (2013).

© 2017 Nature America, Inc., part of Springer Nature. All rights reserved.

ONLINE METHODS

Cell cultures. C2C12 mouse skeletal myoblasts (ATCC; CRL-1772) and NIH/3T3 mouse fibroblasts (ATCC; CRL-1658) were grown in Dulbecco's modified Eagle's medium (DMEM) (4.5 g/l D-glucose and glutamax) (GIBCO) and 10% fetal bovine serum (FBS; Sigma) with penicillin-streptomycin supplement, according to standard protocols. We differentiated C2C12 myoblasts at 90–95% confluence in DMEM and 2% horse serum (Euroclone) with penicillin-streptomycin supplement. Human primary myoblasts (provided by Marina Mora, "Cells, tissues and DNA from patients with neuromuscular diseases" Telethon Biobank) were cultured in DMEM supplemented with 20% FBS, 10 mg/ml insulin, 25 ng/ml human fibroblast growth factor, 10 ng/ml human epidermal growth factor (proliferation medium). We induced the differentiation of human primary myoblasts at 70–80% confluence by adding DMEM supplemented with 2% horse serum (differentiation medium). The cell lines were periodically tested for mycoplasma contamination.

Cell treatments, siRNA and plasmid transfection. To test atrophic stimulation, we treated day-1 myotubes with 100 μM H_2O_2 (Sigma) or 100 μM $FeSO_4$ (Sigma) for 24 h. In the hypertrophic stimulation, day-2 myotubes were heat-shocked at 43 °C for 1 h and then maintained at 37 °C for 1.5 h before collection. To control atrophy induction, we evaluated the gene expression levels of *Atrogin1*; to control hypertrophy induction, we evaluated the gene expression levels of *Hsp70* (*Hspa1b*). We evaluated myosin and myogenin protein content to control atrophy and hypertrophy induction. In the C2C12 recovery experiment, after H_2O_2 treatment, the medium was replaced with fresh differentiation medium, and cells were collected after 48 h. For proteasome inhibition, day-2 myotubes were contemporaneously treated with 10 μM MG132 (Sigma) and 100 μM H_2O_2 (Sigma) for up to 10 h. In the knockdown experiments, Eed knockdown was done as described in ref. 40; for Ezh1 knockdown, 20 nM duplex siRNA was delivered on confluent myoblasts at the time of differentiation induction, and the experiment was repeated after 24 h in differentiating myotubes according to the manufacturer's protocol (Dharmafect 3 reagent; Dharmacon). siRNA oligo sequences are listed in **Supplementary Table 2**; a mix of oligos 1 and 2 was used. In the stable C2C12 cell line overexpressing HA-tagged Ezh1α, we transfected myoblasts with pCDNA-4TO-Ezh1α-HA plasmid (kindly provided by Raphael Margueron), using Lipofectamine 2000 (Invitrogen) according to the manufacturer's instructions. Stable clones were selected in zeocin (250 μg/ml) for 30 d. Transient transfections were carried out with Lipofectamine 2000 or Lipofectamine 3000 (Invitrogen) according to the manufacturer's instructions.

FACS analysis and sorting. In the cell-vitality analysis, 10^6 cells were collected with trypsin, washed with cold phosphate-buffered saline (PBS), suspended in 0.1 ml of cold PBS, fixed by drop-by-drop addition of 1 ml of 70% cold ethanol, and incubated for 1 h on ice. The cells were then washed with PBS, suspended in 1 mg/ml RNase A in PBS, and left for 30 min at 37 °C. The cells were incubated with 20 mg/ml propidium iodide for 30 min in the dark at 4 °C. The cells were analyzed for DNA content with a BD FACS instrument. To sort the mock (empty vector)-YFP, Ezh1β-YFP- and Eed-CFP-positive cells, we collected transiently transfected cells with trypsin, washed them in cold PBS, suspended them in 0.1 ml of cold PBS, and sorted them with a FACSAria cell sorter.

Plasmids. Ezh1β was amplified from C2C12 myotube cDNA and cloned in a pET15b (Novagen) vector modified with 3× Flag tag at the C terminus for GST pull-down, in pcDNA5TO (Invitrogen) or pcDNA5TO-YFP (YFP at the N terminus) for FRET, and in pNLF1-N (Promega) for the NanoLuc assay. Ezh1α was cloned in empty pcDNA5TO (Invitrogen) or pcDNA5TO-YFP (YFP at the N terminus) for FRET. Eed was cloned in the pGex-4T gene fusion system (GE Healthcare) for GST pulldown, in pE-CFP C1 backbone (Clontech) for FRET, and in pNLF1-N (Promega) for the NanoLuc assay. Suz12 was cloned in the pGex-4T gene fusion system (GE Healthcare) for GST pulldown. YFP/CFP-fused proteins were cloned in pcDNA5TO backbone. Details are available from the corresponding author upon request.

RNA isolation and RT-qPCR. Total RNA was isolated with Tri-reagent (Sigma) according to the manufacturer's instructions. Mouse tissues were isolated and homogenized, and RNA was extracted in Trizol with a Qiagen Tissue Ruptor. cDNA was produced starting at 1 μg of RNA from each sample with a Quantitect reverse-transcription kit (Qiagen) or with a Superscript III first-strand cDNA synthesis system (Thermo Fisher) and analyzed in Syber Green-qPCR assays (Applied Biosystems). Real-time PCR analyses were carried out with a Rotor-Gene Q thermal cycler (Qiagen) or with One-step Plus (Life Technologies). The primer sequences are provided in **Supplementary Table 2**.

Protein and histone extraction. We prepared nuclear and cytosolic extracts by lysing cells with cytosolic extraction buffer (10 mM HEPES KOH, pH 8.5, 10 mM NaCl, 0.1 mM EDTA, 0.1 mM EGTA, 1 mM DTT, 1× protease inhibitor, NP-40 0.5%). Nuclei were collected at 1,500*g* and 4 °C, washed three times with equal amounts of cytosolic extraction buffer without NP-40, and resuspended in nuclear extraction buffer (20 mM HEPES KOH, pH 8.5, 400 mM NaCl, 0.1 mM EDTA, 0.1 mM EGTA, 1 mM DTT). The nuclear extracts were then sonicated. Nuclear and cytosolic extracts were collected after debris sedimentation at 16,300*g* and 4 °C, for 10 min. We prepared total extracts by lysing cells in total extraction buffer (50 mM Tris-HCl, pH 8, 150 mM NaCl, 1% NP-40, 1× protease inhibitor) and then carrying out sonication and sedimentation at 16,300*g* and 4 °C, for 10 min. We prepared histone extracts by lysing cells in cytosolic extraction buffer (10 mM HEPES KOH, pH 8, 10 mM KCl, 0.1 mM $MgCl_2$, 0.1 mM EDTA, 0.1 mM DTT, 1× protease inhibitor). The nuclei were collected at 1,500*g* and 4 °C, washed three times with equal amounts of cytosolic extraction buffer, and resuspended in 0.2 N HCl overnight at 4 °C on the wheel. Histone extracts were collected after debris sedimentation at 16,300*g* and 4 °C, for 10 min. To prepare muscle tissue histone extracts, we homogenized muscle slices in 15 mL of ice-cold lysis buffer (250 mM sucrose, 200 mM NaCl, 10 mM Tris-HCl, pH 8.2, 0.1 mM $MgCl_2$, 1 mM $CaCl_2$, 1% Triton X-100, 1 mM PMSF) with a tight-fitting pestle. Nuclei were recovered by centrifugation at 375*g* and 4 °C for 10 min, suspended in 500 μl of 0.4 N NH_2SO_4, and incubated for 30 min on ice. Acid-extracted nuclei were sedimented at 18,400*g* and 4 °C for 10 min, after which 400 μl of supernatant was taken up and mixed with 60 μl of 1 M Tris-HCl, pH 8.0, and 40 μl of 10 N NaOH. Core histones were solubilized by perchloric acid (4% final concentration) and incubated overnight at 4 °C. Samples were centrifuged at maximum speed (21,130*g*) at 4 °C for 1 h and washed twice with 4% perchloric acid, twice with acetone containing 0.2% HCl, and twice with 100% acetone, with 5 min of centrifugation at the maximum speed (21,130*g*) at 4 °C between steps. The pellets were air-dried for 20 min, suspended in H_2O, and diluted in 5× Laemmli loading buffer in which the pH was equilibrated with NaOH. Protein extracts were quantified with a Qubit (Invitrogen) fluorometer or by Bradford assay and used for subsequent western blotting analysis. A list of antibodies used is provided in **Supplementary Table 2**.

Coimmunoprecipitation. For the co-IP experiments, 30×10^6 pelleted cells were suspended in 6 mL of cytosolic extraction buffer (50 mM Tris-HCl, pH 8, 150 mM NaCl, 0.5 mM EDTA, 10 mM imidazole, pH 8, 0.5% Triton X-100, 5% glycerol). The nuclei were pelleted at 1,500*g* and 4 °C, and the supernatant was used for cytosolic IP. Nuclei were washed once in cytosolic extraction buffer and suspended in 3 ml of nuclear extraction buffer (50 mM Tris-HCl, pH 8, 50 mM NaCl, 0.5 mM EDTA, 10 mM imidazole, pH 8, 0.5% Triton X-100, 5% glycerol), sonicated and digested with DNase (75 U of Turbo DNase (Ambion)). Debris was pelleted at 16,380*g* and 4 °C, and the supernatant was used for nuclear IP. Alternatively, 30×10^6 pelleted cells were suspended in 6 mL of extraction buffer (50 mM Tris-HCl, pH 8, 150 mM NaCl, 0.5 mM EDTA, 10 mM imidazole, pH 8, 0.5% Triton X-100, 5% glycerol), sonicated and digested with DNase (75 U of Turbo DNase (Ambion)). Debris was pelleted at 16,380*g* and 4 °C, and the supernatant was used for total IP. Each IP was set up with 2 mg of protein in a final volume of 600 μl at a final concentration of 150 mM NaCl; then 6–8 μg of the appropriate antibodies were added and incubated overnight at 4 °C on the wheel. The immunocomplexes were then recovered with 80 μL (1/10 of IP volume) of magnetic Dynabeads (protein A/G; Invitrogen) and washed with wash buffer (50 mM Tris-HCl, pH 8, 200 mM NaCl, 0.5 mM EDTA, 10 mM imidazole, pH 8, 0.5% Triton X-100, 5% glycerol) four times for 5 min with rotation at 4 °C. Bead elution was done with 400 mM TE buffer (10 mM Tris-HCl, pH 8, 1 mM EDTA, 400 mM NaCl) at 55 °C for 30 min or in elution buffer at 95 °C for 5 min (5% SDS, 10 mM DTT). The eluted immunoprecipitates were loaded on polyacrylamide or Bolt Bis-Tris (Invitrogen) gel and subjected to western blotting analysis. A list of antibodies used is provided in **Supplementary Table 2**.

© 2017 Nature America, Inc., part of Springer Nature. All rights reserved.

Western blotting and densitometry-quantification analysis. For the western blotting analysis, we optimized the quantity of proteins loaded on polyacrylamide gels to avoid signal saturation. The range chosen was 0.5–5 µg for histones and 5–20 µg for non-histone proteins. High-abundance proteins used as loading controls were diluted from 1:10 to 1:20 relative to other proteins. To appreciate Eed relocalization in the nuclear-cytosolic compartments after oxidative stress (**Fig. 4a**), we blotted Eed in both concentrated and diluted conditions (in **Fig. 4a** we refer to the latter condition as "1:20"). Proteins were resolved by SDS-PAGE with 8%, 12% or 4–12% gels (homemade gels or Bolt Bis-Tris (Invitrogen)), depending on the protein mass, and transferred to a nitrocellulose membrane (wet transfer or iBlot Dry Blotting system (Invitrogen)). The membrane was blocked and incubated overnight at 4 °C with primary antibodies. Then it was treated with the appropriate secondary antibody coupled to HRP and revealed through chemiluminescence using a West Dura kit (Pierce, Rockford, USA). Bands were visualized by autoradiography with X-ray films or through a light-sensitive CCD (charge-coupled device) camera (Las 3000) with a linear response to the emitted light. Densities of protein bands were measured with ImageJ software (http://imagej.nih.gov/ij/) using the tool "Analize - Gel - Select lane - Plot lane." The results were normalized to an internal loading control and expressed in terms of fold enrichment relative to the control sample. In an effort to be quantitative, we also ran and quantified western blots for histones in an optimized way (**Supplementary Fig. 1f**,**g**): the samples were loaded in triplicate on the same gel, transferred to a nitrocellulose membrane, incubated overnight at 4 °C with primary antibodies followed by the appropriate fluorescent-conjugated secondary antibodies (IRDye 800 goat anti-rabbit, IRDye 680 goat anti-mouse), and revealed through STARION FLA 9000 (Fujifilm). This system guarantees a linear signal response and provides sensitive and precise quantification. In this case, quantification of the bands was calculated with the Image Reader FLA 9000 software; the results were normalized to an internal loading control and expressed in terms of fold enrichment relative to the control sample. A list of primary antibodies used for western blotting and the corresponding conditions is provided in **Supplementary Table 2**.

Histone methyl transferase activity. We optimized the assay by testing different concentrations of Ezh1 antibody (from the Margueron lab) (Ezh1i, 4 µl; Ezh1ii, 8 µl), and then we used the concentration with the best performance (Ezh1ii) for the assay (**Supplementary Fig. 2a**). We also carried out Suz12 IP as an additional control for the co-IP experiment. To measure HMTase activity, we used a commercial colorimetric kit according to the manufacturer's instructions (Epigentek). We carried out IP for Ezh1 and Ezh2 in nuclear extracts of control and H_2O_2-treated myotubes; eluted immunoprecipitates were quantified with Qbit, and serial dilutions were tested for HMTase activity. For the quantitative assay, we chose to use 300 ng of immunoprecipitated HMTase enzymes (Ezh1 or Ezh2). We then calculated the HMT activity by reading the absorbance of the assay (OD). A list of antibodies used for IP is provided in **Supplementary Table 2**.

Chromatin immunoprecipitation. Cells were cross-linked in 1% formaldehyde (Sigma). Cross-linked cells were lysed in lysis buffer 1 (50 mM HEPES KOH, pH 7.5, 10 mM NaCl, 1 mM EDTA, 10% glycerol, 0.5% NP-40, 0.25% Triton X-100). Nuclei were collected, washed in lysis buffer 2 (10 mM Tris-HCl, pH 8, 200 mM NaCl, 1 mM EDTA, 0.5 mM EGTA) and lysed in lysis buffer 3 (10 mM Tris-HCl, pH 8, 100 mM NaCl, 1 mM EDTA, 0.5 mM EGTA, 0.1% Na-deoxycholate, 0.5% N-laurylsarcosine). Lysis buffers were complemented with 1× proteinase inhibitor cocktail. Chromatin was sheared (BRANSON A250 with a 3.2-mm tapered microtip; four cycles of 1.5 min at 20% amplitude, 50% of duty cycle) and checked on 0.9% agarose gel run at 70 V. In each IP reaction, 100 µg of chromatin DNA equivalents (DNA concentration read at Nanodrop) were incubated overnight with 5–8 µg of antibodies. The immunocomplexes were recovered with magnetic Dynabeads (protein G; Invitrogen) for 2 h and washed on the wheel at 4 °C for 5 min with low-salt (LS) wash buffer (0.1% SDS, 2 mM EDTA, 1% Triton X-100, 20 mM Tris-HCl, pH 8, 150 mM NaCl), then high-salt (HS) wash buffer (0.1% SDS, 2 mM EDTA, 1% Triton X-100, 20 mM Tris-HCl, pH 8, 500 mM NaCl), then LS wash buffer (wash buffers were complemented with proteinase inhibitor cocktail), and then washed briefly in TE 150 mM NaCl and resuspended in elution buffer (50 mM Tris-HCl, pH 8, 10 mM EDTA, 1% SDS) for de-cross-linking overnight at 65 °C. Chromatin was digested with RNase A (0.2 mg/ml) and proteinase K (0.2 mg/ml), and DNA was purified for qPCR analysis. ChIP results are expressed as fold enrichment over the mock condition. ChIP results for H3K27me3 are also expressed as the percentage of immunoprecipitated histone H3. A list of antibodies used is provided in **Supplementary Table 2**.

RNA-seq and ChIP-seq data generation and analysis. Total RNA was used for library preparation for Illumina sequencing with a TruSeq standard total RNA kit or TruSeq RNA kit. Replicates were sequenced on a HiSeq-2000. RNA-seq data in control and H_2O_2-treated myotubes were collected; three biological replicates were available for each data set. The quality control of the reads was evaluated with FastQC software (http://www.bioinformatics.babraham.ac.uk/projects/fastqc/), and then the reads were trimmed with the Trimmomatic tool[41]. The FASTQ files were mapped to mouse reference genome GRCm38/mm10 with STAR v.2.2.0 (ref. 42), and gene-expression levels were assessed by Cufflinks 2.2.1 (ref. 43). All parameters were set up according to the default settings of STAR and Cufflinks. Finally, we carried out a differential expression analysis with Cuffdiff 2.2.1, using upper-quartile normalization (–library-norm-method quartile). The genes with $P < 0.05$ and with a fold-change (untreated/treated) cutoff of 2 were considered as differentially expressed genes in the downstream analysis. ChIP-seq data were collected in control and H_2O_2-treated myotubes immunoprecipitated for Eed (one replicate), Suz12 (one replicate) and Ezh1α (two replicates). ChIP-seq data quality control and trimming (50-cycle single-read) were done as for RNA-seq. The FASTQ files were mapped to the mouse genome (GRCm38/mm10 version) with Bowtie2 software[44] with the "very sensitive" option. Multi-alignments and duplicate reads were removed with SAMtools[45], and filtered mapped reads were the input for the peak-detection step. Tags mapped to enriched regions were detected with the SICER algorithm[46]. Input DNA was used in the peak-calling step to remove background noise. A window size of 200 bp and a gap size of 600 bp were set for the detection of enriched islands. Finally, only statistically significantly enriched regions (FDR < 0.01) were considered for peak annotation by the ChIPseeker package[47].

RNA-seq and ChIP-seq downstream analysis and integration. The common ChIP-seq peaks called for Eed, Suz12 and Ezh1α in control and H_2O_2-treated myotubes were considered for downstream analysis (**Supplementary Fig. 3b**). We used Qiagen's Ingenuity Pathway Analysis (http://www.qiagen.com/ingenuity) to analyze PRC2–Ezh1 gene targets in control (494 genes) and H_2O_2-treated myotubes (826 genes) (**Fig. 2a**). Network results were considered according to the significance score and were represented in relation to the subcellular localization of the genes and the inter- and intra-networks of the functional relationships. Through RNA-seq differential expression analysis, we found 318 genes that were downregulated in H_2O_2-treated myotubes with respect to the control condition; we compared these genes with Eed, Suz12, and Ezh1 target genes in H_2O_2-treated myotubes and found that 224 out of the 318 downregulated genes were also targeted by these proteins after H_2O_2 treatment. We then carried out a GO enrichment analysis on these 224 genes, using the FatiGO tool in the Babelomics suite (version 5)[48], considering only GO terms with an adjusted P value less than 0.05, which resulted in 141 GO terms. We carried out a GO semantic similarity analysis on those terms with the GOssTO tool[49]. That analysis provided a symmetric matrix in which each value represented a score of similarity between GO term pairs; we then carried out hierarchical clustering based on the semantic similarity matrix to identify the representative clusters. We confirmed the presence of GO term clusters with the REVIGO webtool[50] and identified six representative terms.

Fluorescence resonance energy transfer assay. NIH/3T3 cells faintly express endogenous Ezh1β. We optimized the transfection of these cells so as to produce an amount of Ezh1β-YFP analogous to the amount of endogenous Ezh1β in C2C12 myotubes (data not shown). NIH/3T3 cells were cotransfected with fluorescence-tagged proteins in an adjusted stoichiometric ratio (8:1 Eed-CFP:YFP, Eed-CFP:Ezh1α/β-YFP or Eed-CFP:Ezh2) to optimize the protein distribution. Alternatively, for competition assays, cells were cotransfected so as to maintain the established ratio and with an increasing amount of 'cold' (not tagged) Ezh1α or Ezh1β. Ezh1β-YFP or Ezh1α-YFP was cotransfected with cold Ezh1α or Ezh1β, respectively, at 1:0, 1:0.5 or 1:1. The cells were then fixed in 2% paraformaldehyde for 10 min at room temperature. Images were taken with a Leica TCS SP5 confocal microscope with an HCX PL APO 63.0×/1.40-NA (numerical aperture) oil-immersion objective and 8× zoom. We used the argon laser to excite

© 2017 Nature America, Inc., part of Springer Nature. All rights reserved.

doi:10.1038/nsmb.3392

CFP at 458 nm (intensity of 11%), and we measured emission in the range of 464–498 nm. We excited YFP at 514 nm (intensity of 3%) and measured emission between 531 and 566 nm. We analyzed FRET acceptor photobleaching with the FRET AB software (Leica); the region of interest was bleached with the 514-nm laser at full power. FRET efficiency was calculated as $(D_{post} - D_{pre})/D_{post}$, where D_{post} is the fluorescence intensity of the donor after acceptor photobleaching, and D_{pre} is the fluorescence intensity of the donor before acceptor photobleaching. $N = 30$ from three different biological experiments.

Recombinant protein purification and GST pulldown experiments. Recombinant proteins for pulldown experiments were produced and purified from *Escherichia coli* strain BL21DE. The bacterial pellet of His-Ezh1β-3×Flag was resuspended in lysis buffer (300 mM NaCl, 50 mM Na_2HPO_4, 5% glycerol, 0.5% Triton X-100, 1× proteinase inhibitor), incubated for 30 min under gentle shaking at 4 °C, sonicated for 10 min (Bioruptor sonicator; Diagenode) and centrifuged for 10 min at 20,000*g* at 4 °C. The supernatant was loaded on anti-Flag M2 affinity gel (Sigma; A2220), incubated overnight at 4 °C, washed with TBS at a volume equal to ten times the total packed gel volume, and eluted with TBS containing 100 μg/ml Flag peptide. Eed-GST and Suz12-GST recombinant protein was purified as follows: the bacterial pellet was resuspended in lysis buffer (PBS, pH 7.4, 150 mM NaCl, 10 mM Na_2HPO_4, 5 mM EDTA, 0.1% TritonX-100, 1× proteinase inhibitor), incubated for 30 min at 4 °C with agitation, sonicated for 10 min, and centrifuged for 10 min at 12,000*g* at 4 °C. The supernatant was loaded onto a GST column (GST Trap FF; GE Healthcare), washed with five column volumes of wash buffer (PBS, pH 7.4, 150 mM NaCl, 10 mM Na_2HPO_4, 5 mM EDTA) and eluted with GST elution buffer (50 mM Tris-HCl, pH 8, 10 mM GSH). For pulldown purposes, 1 μg of purified Eed-GST or Suz12-GST was incubated with magnetic beads (Invitrogen; 1004D) conjugated with 1 μg of anti-GST (sc-138; Santa Cruz Biotechnology) overnight at room temperature under gentle shaking. The beads were washed twice with binding buffer (TBS, 200 mM KCl, 0.1% NP-40, 5 mM β-mercaptoethanol, protease inhibitor cocktail) and then incubated with 1 μg of His-Ezh1β-3×Flag in the same buffer for 2 h at 4 °C. After three washes in binding buffer, the interacting proteins were eluted in loading buffer by heating at 95 °C and were analyzed by immunoblotting.

NanoLuc assay. For the NanoLuc assay, 100 ng of Ezh1β-NanoLuc and Eed-NanoLuc plasmids were transfected with Lipofectamine 3000 according to the manufacturer's instructions on C2C12 and NIH/3T3 cells seeded in 96-well micro-plates for luminescence assays; 36 h after transfection, the cells were treated with H_2O_2. The luminescence assay was carried out with NanoGlo Luciferase assay reagent according to the manufacturer's instructions.

Unilateral hindlimb immobilization and histology. Mice were bred and maintained according to the standard animal facility procedures. All experimental protocols were approved by the internal Animal Research Ethical Committee according to standards of the Italian Ministry of Health and complying with the NIH Guide for the Care and Use of Laboratory Animals. One hindlimb of each of three 3-month-old C57BL/6 female mice was immobilized with two plastic sticks. The sticks were covered with cotton adhesive bands to prevent lesions, placed over and under the limb, and fixed with a medical adhesive band; the foot was positioned in plantar flexion to induce maximal atrophy of the lower hindlimb muscles. The animals were free to move, eat and drink *ad libitum*. After 11 d, the mice were killed and the extensor digitorum longus and tibialis anterior muscles were removed from both hindlimbs; because the immobilization procedure exclusively prevented movement of the immobilized leg, the contralateral, non-immobilized leg was used as an internal control for the procedure[20]. Reloaded animals after cast removal were allowed to move freely for 24 d before being killed. Mice were anesthetized with an intraperitoneal injection of a mixture of zolazepam-tiletamine (80 mg/kg; Zoletil 50, Virbac, France) and xylazine (20 mg/kg; Rompun, Bayer HealthCare, Germany). Extensor digitorum longus muscles were used for RNA extractions and analysis. Tibialis anterior muscles were embedded in OCT matrix and snap-frozen in liquid-nitrogen-cooled isopentane. The muscles were cut transversally into cryosections (8 μm) with a Leica CM 3050 S cryostat. Cryosections were fixed in 4% PFA for 15 min and permeabilized with 100% methanol for 6 min at −20 °C. To avoid unspecific binding, muscle sections were first blocked with a solution containing 4% IgG fraction-free BSA in PBS and then with an anti-mouse Fab fragment (Jackson, 1:100). Primary antibody staining was carried out overnight at 4 °C in a 4% BSA solution, and secondary antibody staining (secondary antibodies were coupled to Alexa Fluor 488 or Alexa Fluor 594 (Invitrogen)) was carried out at room temperature in a 4% BSA solution (dilution of 1:1,000). Nuclei were counterstained with 1 μg/ml DAPI. Primary antibodies were used in the following dilutions: H3K27me3 (Millipore; 07-449), 1:100; caveolin 3 (BD Bioscience; 610420), 1:500; laminin (Sigma; L9393), 1:100. Images were acquired with a Zeiss LSM700 confocal microscope and edited with ZEN09 and Photoshop CS6 software.

Immunofluorescence and *in situ* proximity ligation assay. Myotubes treated or not treated with H_2O_2 were fixed with 4% PFA for 15 min, permeabilized with 0.1% Triton X-100 in PBS for 10 min, and blocked with 1% BSA solution. Primary antibody staining was carried out overnight at 4 °C in a 1% BSA solution at dilutions of 1:800 for Suz12 (Cell Signaling; DR9F6 XP) and 1:250 for Eed (Millipore; 051320). Secondary antibody staining was carried out at room temperature in a 1% BSA solution (1:1,000). Secondary antibodies were coupled to Alexa Fluor 488 or Alexa Fluor 568 (Invitrogen). Nuclei were counterstained with 1 μg/ml DAPI. Images were obtained with a Leica TCS SP5 confocal microscope with an HCX PL APO 63.0×/1.40-NA oil-immersion objective. Proximity ligation assay (PLA Duolink DUO92014, DUO92005, DUO92001) was carried out according to the manufacturer's instructions. Nuclei were counterstained with 1 μg/ml DAPI. Images were obtained with a Nikon Wildefield microscope 63× objective. The fluorescence mean intensities for H3K27me3 immunostaining on tibialis sections were calculated with ImageJ software. For each field, the software automatically selected areas stained with DAPI for the selected area for the ImageJ "RGB profiler" plugin measure: the red, green and blue mean fluorescence intensity. Eed and Suz12 immunofluorescence was analyzed with the Volocity software, with the following pipeline used for each 3D-reconstructed field: Nuclei selection in DAPI channel - Calculate colocalization – Calculate Cytoplasm_Invert nuclei _excluding object<1000 μm^3. In this way, for each identified nucleus, the fluorescence mean intensities of Eed and Suz12 and their colocalization (global Pearson correlation values) were evaluated; we evaluated Eed and Suz12 cytosolic mean intensities by subtracting nuclei signals from the global field mean intensity. Multiple nuclei in close proximity, otherwise considered as a single object, were discarded, which introduced a cutoff that excluded objects with a volume less than 100 μm^3 and greater than 500 μm^3. Proximity ligation assay mean fluorescent intensities for each nucleus were evaluated by Volocity according to the analog parameters.

Statistics and reproducibility. In bar graphs, values are mean and s.e.m.; where $n = 2$, data are presented as individual points. Box-and-whisker plots show the median, ±1.5× the IQR, and the 25% and 75% quantiles. Numbers of replicates are indicated in figure legends. To determine the significance between two groups, we made comparisons by appropriated Student's *t* test; exact *P* values and exact types of tests used are specified in figure legends. For correlation analysis, the Z-Fisher test was used; the exact values are specified in the legends. Multiple comparisons were done by univariate ANOVA to compare more than two means; exact *P* values, types of tests used, and *F* values are specified in figure legends. For all statistical tests, the 0.05 level of confidence was accepted for statistical significance. For all ANOVAs and *t* tests, degrees of freedom correspond to $N - 1$, where N is the sample size. For animal experiments, no statistical method was used to predetermine sample size, and the experiments were not randomized and were not performed with blinding.

Data availability. Data that support the findings of this study are available in ArrayExpress under accession codes E-MTAB-3194 for RNA-seq data and E-MTAB-4794 for ChIP-seq data. Source data for **Figures 1** and **3–6** and for **Supplementary Figures 1**, **2** and **4–6** are available online. Other data are available from the corresponding author upon request.

40. Cesarini, E. *et al.* Lamin A/C sustains PcG protein architecture, maintaining transcriptional repression at target genes. *J. Cell Biol.* **211**, 533–551 (2015).
41. Bolger, A.M., Lohse, M. & Usadel, B. Trimmomatic: a flexible trimmer for Illumina sequence data. *Bioinformatics* **30**, 2114–2120 (2014).
42. Dobin, A. *et al.* STAR: ultrafast universal RNA-seq aligner. *Bioinformatics* **29**, 15–21 (2013).
43. Trapnell, C. *et al.* Transcript assembly and quantification by RNA-seq reveals unannotated transcripts and isoform switching during cell differentiation. *Nat. Biotechnol.* **28**, 511–515 (2010).

© 2017 Nature America, Inc., part of Springer Nature. All rights reserved.

44. Langmead, B. & Salzberg, S.L. Fast gapped-read alignment with Bowtie 2. *Nat. Methods* **9**, 357–359 (2012).
45. Li, H. A statistical framework for SNP calling, mutation discovery, association mapping and population genetical parameter estimation from sequencing data. *Bioinformatics* **27**, 2987–2993 (2011).
46. Xu, S., Grullon, S., Ge, K. & Peng, W. Spatial clustering for identification of ChIP-enriched regions (SICER) to map regions of histone methylation patterns in embryonic stem cells. *Methods Mol. Biol.* **1150**, 97–111 (2014).
47. Yu, G., Wang, L.G. & He, Q.Y. ChIPseeker: an R/Bioconductor package for ChIP peak annotation, comparison and visualization. *Bioinformatics* **31**, 2382–2383 (2015).
48. Alonso, R. *et al.* Babelomics 5.0: functional interpretation for new generations of genomic data. *Nucleic Acids Res.* **43**, W117–W121 (2015).
49. Caniza, H. *et al.* GOssTo: a stand-alone application and a web tool for calculating semantic similarities on the Gene Ontology. *Bioinformatics* **30**, 2235–2236 (2014).
50. Supek, F., Bošnjak, M., Škunca, N. & Šmuc, T. REVIGO summarizes and visualizes long lists of gene ontology terms. *PLoS One* **6**, e21800 (2011).

© 2017 Nature America, Inc., part of Springer Nature. All rights reserved.

 doi:10.1038/nsmb.3392